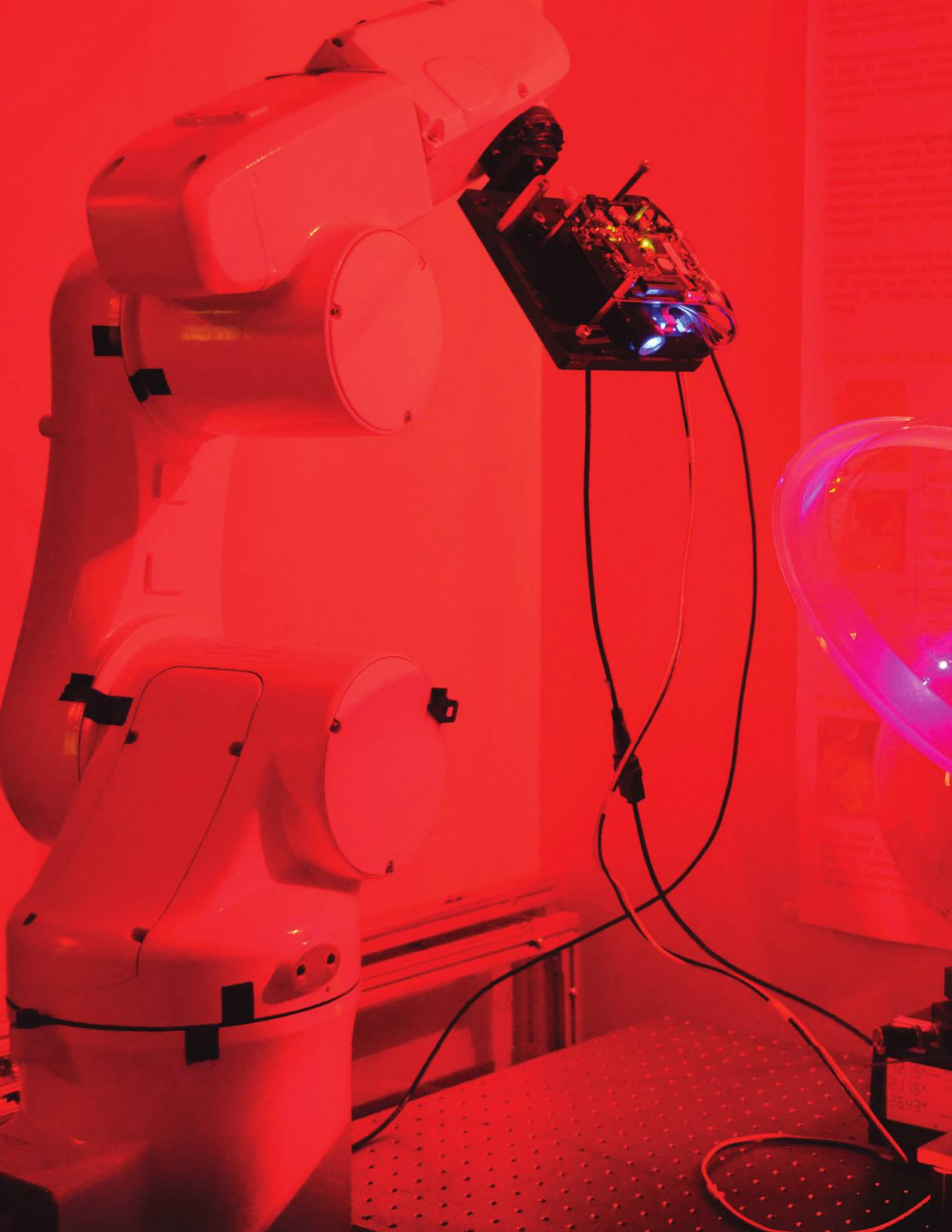

3D PRINTING AND ADDITIVE MANUFACTURING
Volume 3, Number 4, 2016

DOI: 10.1089/3dp.2016.0042

ORIGINAL ARTICLE

Conformal Robotic Stereolithography

Adam G. Stevens,[1,2,*] C. Ryan Oliver,[1,2,*] Matthieu Kirchmeyer,[1,3] Jieyuan Wu,[1] Lillian Chin,[1] Erik S. Polsen,[2] Chad Archer,[2] Casey Boyle,[2] Jenna Garber,[2] and A. John Hart[1,2]

Abstract

Additive manufacturing by layerwise photopolymerization, commonly called stereolithography (SLA), is attractive due to its high resolution and diversity of materials chemistry. However, traditional SLA methods are restricted to planar substrates and planar layers that are perpendicular to a single-axis build direction. Here, we present a robotic system that is capable of maskless layerwise photopolymerization on curved surfaces, enabling production of large-area conformal patterns and the construction of conformal freeform objects. The system comprises an industrial six-axis robot and a custom-built maskless projector end effector. Use of the system involves creating a mesh representation of the freeform substrate, generation of a triangulated toolpath with curved layers that represents the target object to be printed, precision mounting of the substrate in the robot workspace, and robotic photopatterning of the target object by coordinated motion of the robot and substrate. We demonstrate printing of conformal photopatterns on spheres of various sizes, and construction of miniature three-dimensional objects on spheres without requiring support features. Improvement of the motion accuracy and development of freeform toolpaths would enable construction of polymer objects that surpass the size and support structure constraints imparted by traditional SLA systems.

Keywords: stereolithography, photopatterning, projection lithography, robotics

Introduction

Among the several widespread additive manufacturing (AM) techniques,[1–5] stereolithography (SLA) is attractive because of its high spatial resolution and diverse materials library, ranging from elastomeric to ceramic materials.[6–9] For example, Align Technologies uses SLA for mass-customized production of millions of dental replicas that are used to mold unique orthodontic aligners,[10] and SLA is used extensively in the film and architecture industries for prototyping of both small-scale and large-scale models and props.[2,11–15] Recent advances in SLA technology include desktop machines that incorporate low-cost lasers and/or digital light projectors (Formlabs Form 2, Nobel 1.0), significantly faster SLA printing achieved by local modulation of oxygen-induced inhibition,[16] and SLA printing of siloxane-based resins that can be converted into ceramics on subsequent heat treatment.[8]

However, traditional SLA machines are, like most AM equipment, designed to build parts on planar reference surfaces and do not easily permit construction on nonplanar substrates. Moreover, the working volume of AM systems, which typically use orthogonal gantry style motion systems,[14] is limited, even though the forces involved in deposition are significantly lower than the forces in conventional machining operations. In the case of SLA,[17] the machine design is also restricted by the requirement to dispense and/or recoat the resin with each layer,[18] and steeply overhanging surfaces of parts must be supported by scaffolds that are often

[1]Department of Mechanical Engineering and Laboratory for Manufacturing and Productivity, Massachusetts Institute of Technology, Cambridge, Massachusetts.
[2]Department of Mechanical Engineering, University of Michigan, Ann Arbor, Michigan.
[3]MINES ParisTech, PSL Research University, Paris, France.
*These authors contributed equally.

Opposite page: The articulated robot arm pauses to expose a section of a conformal pattern on a spherical substrate. With a different end effector and photoresin combination, three-dimensional structures can also be printed on curved substrates.

painstaking to remove and compromise the surface quality of the part.[19]

Industrial robotic manipulators offer a combination of workspace volume, speed, and accuracy that makes them attractive for use in AM processes. For example, a large-scale extrusion AM process referred to as Big Area Additive Manufacturing has been implemented by using both a large six-axis robot and a large-scale gantry system,[20] and it has demonstrated the rapid fabrication of furniture, vehicle components, dwelling structures, and composite tooling.[21] Rapid fabrication of large and complex sand molds by binder jetting has been achieved by using an articulated manipulator to both spread the powder and carry a large inkjet printhead.[22] Also, continuous feed wire welding of materials such as titanium alloys has been used to build large components for aircraft structures and artistic sculptures.[23] These examples show how adaptation of robotic motion systems to the constraints of AM requires simultaneous development of compatible end effectors and software workflows, and an understanding of the system accuracy and its influence on part quality.

We present a system and method for freeform robotic SLA, used both to conformally pattern photopolymers onto curved surfaces and to build three-dimensional (3D) structures on curved substrates. The system combines the advantages of a six-axis robotic arm with a Digital Light Processing (DLP)-based μm-stereolithography (μmSLA) print head end effector and a novel software workflow schema. We discuss the hardware, software, and workflow design for this system; evaluate its positioning accuracy; and present demonstrations of its functionality. The design of a multi-axis μmSLA system is subject to mechanical error, so we discuss the role of error buildup in the system components. Using this prototype system, we demonstrate the patterning of a micro-scale map onto spheres of different length scales, as well as AM of millimeter-scale structures on curved reference substrates.

Materials and Methods

System design and calibration

The system comprises a six-axis articulated robot fitted with a custom-built projection lithography end effector (Fig. 1a). The robot is positioned such that it can project light patterns onto a rotary work stage that holds the build surface and/or the part that serves as the substrate for photopatterning. Operation of the projection system and motion of the robot and rotary stage are synchronized via custom software. Figure 1b presents an overview of the workflow for robotic photopatterning by using the system, which can be configured to photopattern both two-dimensional (2D) (Fig. 1c) and 3D (Fig. 1d) structures with curved layers. This section describes the hardware and software components of each subsystem, as well as the motion system positioning performance.

Photopatterning end effector

The photopatterning end effector (Fig. 2a, b) incorporates a MEMS-based DLP module (Texas Instruments Lightcrafter 4500) into a custom CNC-machined aluminum housing. The DLP module contains an RGB LED light source illuminating the micromirror array, the image of which is, subsequently, projected through an objective lens attached to the housing. The optical path from the blue (exposing) and red (illuminating) LEDs to the substrate and, subsequently, the CCD is shown in Figure 2b. A beamsplitter (Thorlabs CM1-BP108) is placed between the objective and DLP module, enabling the projection to be imaged directly via a CMOS camera in the end effector (Ximea MQ042CG-CM). A long-pass filter (Thorlabs 550) is used to remove the blue exposure light from the beam before imaging with the camera. As shown here, the projector has a 5× objective lens (Mitutoyo), for focusing the DLP image onto the substrate.

The projection system was tested by projecting a modified USAF 1951 test pattern onto a photoresist-coated glass substrate; the USAF 1951 pattern consists of line groups with decreasing line pair distances. After photoresist development, the resulting pattern was measured from SEM images (Fig. 2c). From this, the minimum line pair size in the photoresist (MicroChem MicroSpray™, Positive Photoresist) was measured to be 10 μm. Therefore, we define this value to be the spatial resolution of photopatterning in this end effector configuration.

Motion system and kinematics

The motion system consists of a six-axis articulated robot (Omron Adept Viper s650[24]) combined with a stepper motor-driven rotary stage (Velmex B5990TS), as shown in Figures 1a and 3a. Use of the rotary stage facilitates photopatterning of a larger object with a particular robot work envelope. For example, a large part need only fit into half the work envelope if mounted on a rotary stage, as the stage can be rotated to bring the other half into the work envelope as necessary.

The workpiece is held on a kinematically coupled mount (Thorlabs KB3X3), allowing for rapid, repeatable workpiece positioning in the work envelope after 3D scanning and photopolymer coating. Two orthogonal micrometer stages (Thorlabs PT1A) are mounted between the kinematic mount and the rotary stage to remove runout during calibration of the system. In standard operation, the runout of the rotary stage can be reduced to 12 ± 5 μm, as measured by a dial indicator. The rotary stage introduces an accuracy error of 100 arc-seconds, which amounts to 5 μm at a radius of 10 mm and 50 μm at 100 mm from the center of rotation. Lateral repeatability of the kinematic coupling was evaluated via a touch-probe articulated coordinate measuring machine (CMM, Romer Absolute Arm 7512, Hexagon Metrology), and it was found to be 60 ± 20 μm. For this measurement, a kinematic coupling top plate was fabricated with cylindrical and spherical reference features. The rotary stage is homed by using a magnetic reed switch; its repeatability, measured using the CMM, is ±0.005 degrees, or ~ 0.9 μm at 10 mm and 9 μm at 100 mm from the axis of rotation.

In operation, the end effector and rotary stage must be accurately positioned and oriented, such that the projection plane is both parallel to the local surface of the object and at the requisite focal distance. A kinematic analysis using homogeneous transform matrices (HTMs) is used to understand the propagation of errors through the robot arm and end effector starting at a reference origin (located at the robot base, Fig. 3a) in the workcell. One HTM describes the relationship between each neighboring coordinate frame in a kinematic chain (Fig. 3b), and is composed of four transforms, represented as submatrices: an intrinsic rotation

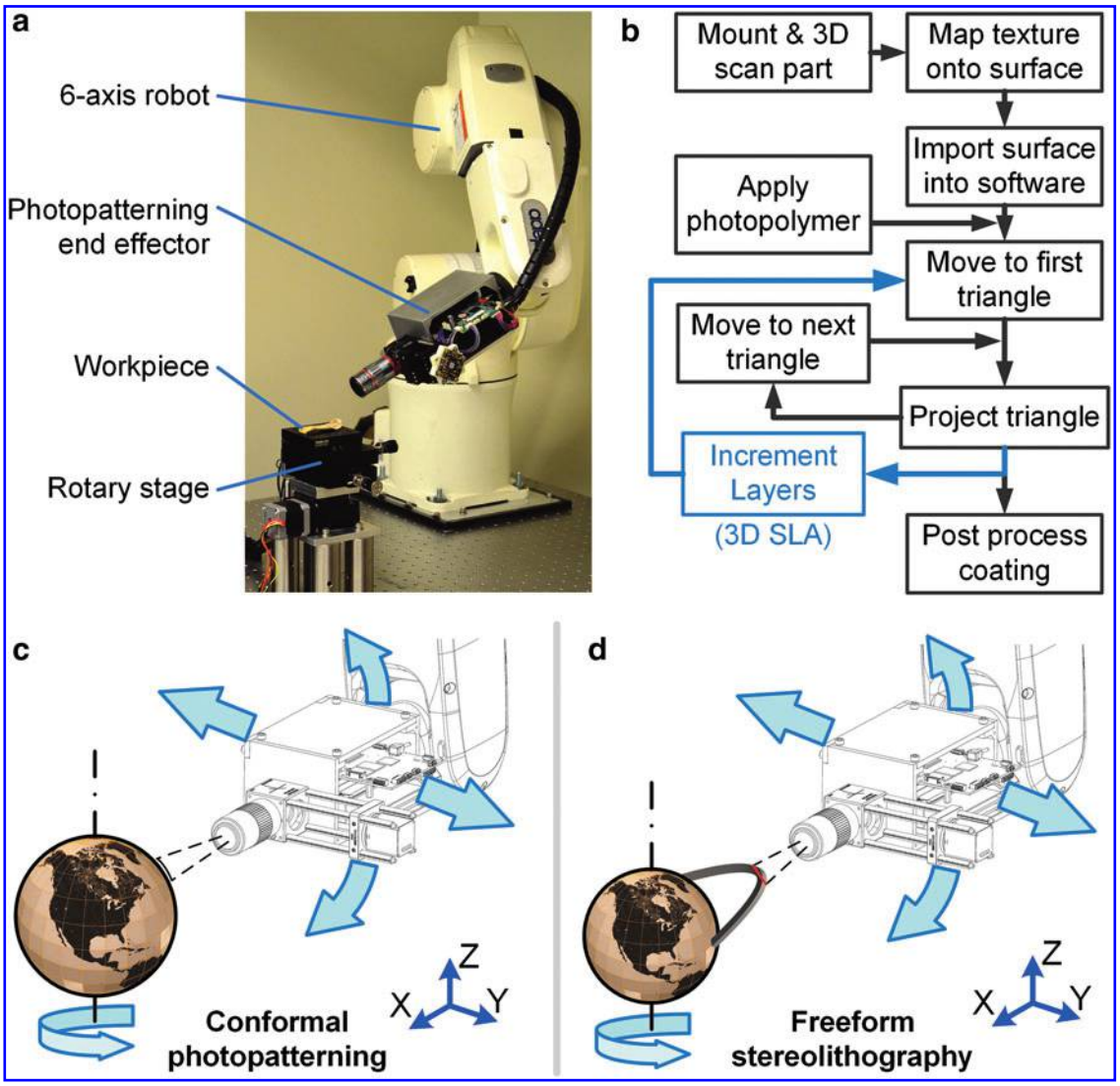

FIG. 1. Robotic sterolithography system: **(a)** overview; **(b)** operation sequence; schematic configurations for **(c)** curved planar photopatterning on freeform substrates such as a spherical substrate; and **(d)** multilayer curved photopatterning of 3D structures such as an arch built from a spherical substrate. 3D, three-dimensional. Color images available online at www.liebertpub.com/3dp

matrix, R_i^{3x3}; translation, L_i^{3x1}; perspective, 0^{1x3}; and scaling, 1.[25] Thus, each HTM is composed as

$$H_i^{i-1} = \begin{bmatrix} R_i^{3x3} & L_i^{3x1} \\ 0^{1x3} & 1 \end{bmatrix} \tag{1}$$

When analyzing a kinematic chain, the perspective and scaling are fixed at 0^{1x3} and 1, respectively.[25]

The total forward kinematic transform for the system, T, relates the origin to the focal plane. This is calculated by the sequential product of all transforms in the kinematic chain (Eq. 2). Consider the Cartesian coordinates of the location of the focal plane in the joint 6 coordinate frame, P^{4x1}, with the fourth row containing the unity scale factor for compatibility with T (Eq. 3). Then, Equation (4) is the description of the end effector location in the origin-centered world coordinates of the robot, constructed from six joint HTMs and a Cartesian offset.

$$T = \prod_{1}^{6} H_i^{i-1} \tag{2}$$

$$P^{4x1} = \begin{bmatrix} x_P \\ y_P \\ z_P \\ 1 \end{bmatrix} \tag{3}$$

$$\begin{bmatrix} x_w \\ y_w \\ z_w \\ 1 \end{bmatrix} = TP^{4x1} \tag{4}$$

By numerically differentiating Equation (4) with respect to the angular position of each joint, the contribution of each joint angle to the motion of the focal plane was calculated

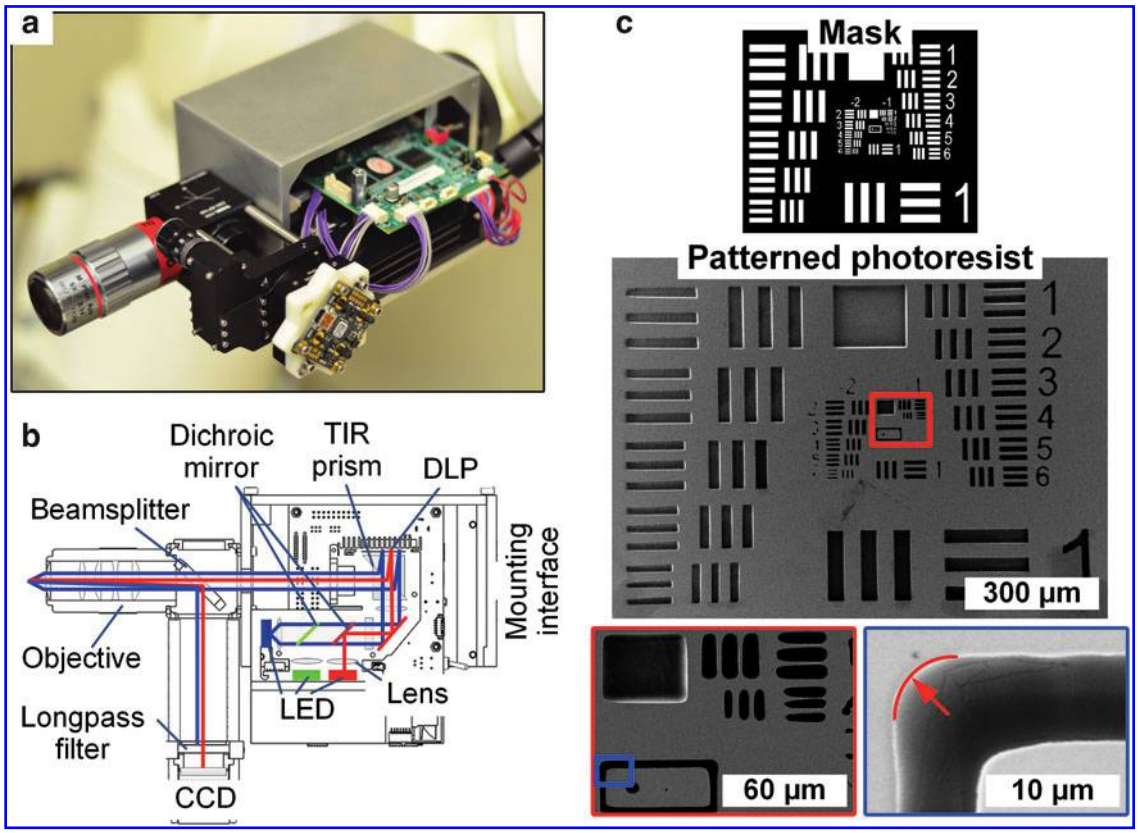

FIG. 2. Dynamic mask projection lithography end effector: **(a)** photograph of optics and custom enclosure mounted to the end of the robot; **(b)** cutaway diagram showing optical path in the end effector; **(c)** images of the modified USAF 1951 resolution test pattern in positive photoresist, compared with digital mask, from which a resolution of 10 μm was defined as the minimum resolved linepair spacing. The minimum radius of curvature is $\sim 5\,\mu$m. Color images available online at www.liebertpub.com/3dp

(Fig. 3c). Higher-numbered joints are closer to the end effector, and as a result are generally associated with lower sensitivities. The error contributions range by $\sim 10^4$-fold; the smallest contribution is due to joint 6 (4.5×10^{-6} mm/°), and the largest is due to joint 1 ($0.67–1.2 \times 10^{-2}$ mm/°). Sensitivity depends on robot pose, giving rise to a range of sensitivities for certain joints. For the data in Figure 3c, a point lattice in front of the workpiece was used to compute the joint sensitivities.

Calibration

To successfully pattern a pre-existing physical surface that has a known digital representation, the position of the surface relative to the motion system must be known. This can be achieved by programming the system software with the coordinates describing the location and orientation of the workpiece in the workspace. These coordinates were measured by CMM using known datum surfaces on the motion system and workpiece.

In addition, when printing patterns on a pre-existing 3D surface with feature sizes approaching the positioning accuracy of the motion system, the robot must have high absolute volumetric accuracy in the workspace relative to a fixed point. This is achievable via calibration if the system repeatability is suitably less than the as-delivered accuracy, which is generally the case for industrial robots.

The positioning repeatability of a tooling ball mounted on the robot end effector was measured via CMM at a collection of robot poses and was found to be $36 \pm 108\,\mu$m (1 standard deviation). This is comparable to the manufacturer specification of 20 μm.[24] The large standard deviation was observed to be due to robot repeatability variation with arm configuration.

However, though highly repeatable, the robotic motion system has only millimeter-level accuracy (Fig. 3d) and, therefore, requires calibration. This was done by using the portable CMM arm in conjunction with several gauging artifacts to create a lookup table of position corrections for a specific workpiece. After correcting for positioning errors, system accuracy is on the order of the measured system repeatability. As will be shown later, the achieved accuracy and measured repeatability have important implications for the system performance when used for conformal photopatterning.

Software and data representation

The software and data representation were developed for the system to operate in both single-layer (conformal 2D patterning) and multilayer (3D patterning) modes. Both modes share the same workflow, except that 3D patterning involves multilayer exposure with incremental delivery of the photopolymer such that a 3D object can be created. As shown in Figure 1b, the operational steps for performing robotic SLA include mounting the workpiece, 3D scanning the workpiece,

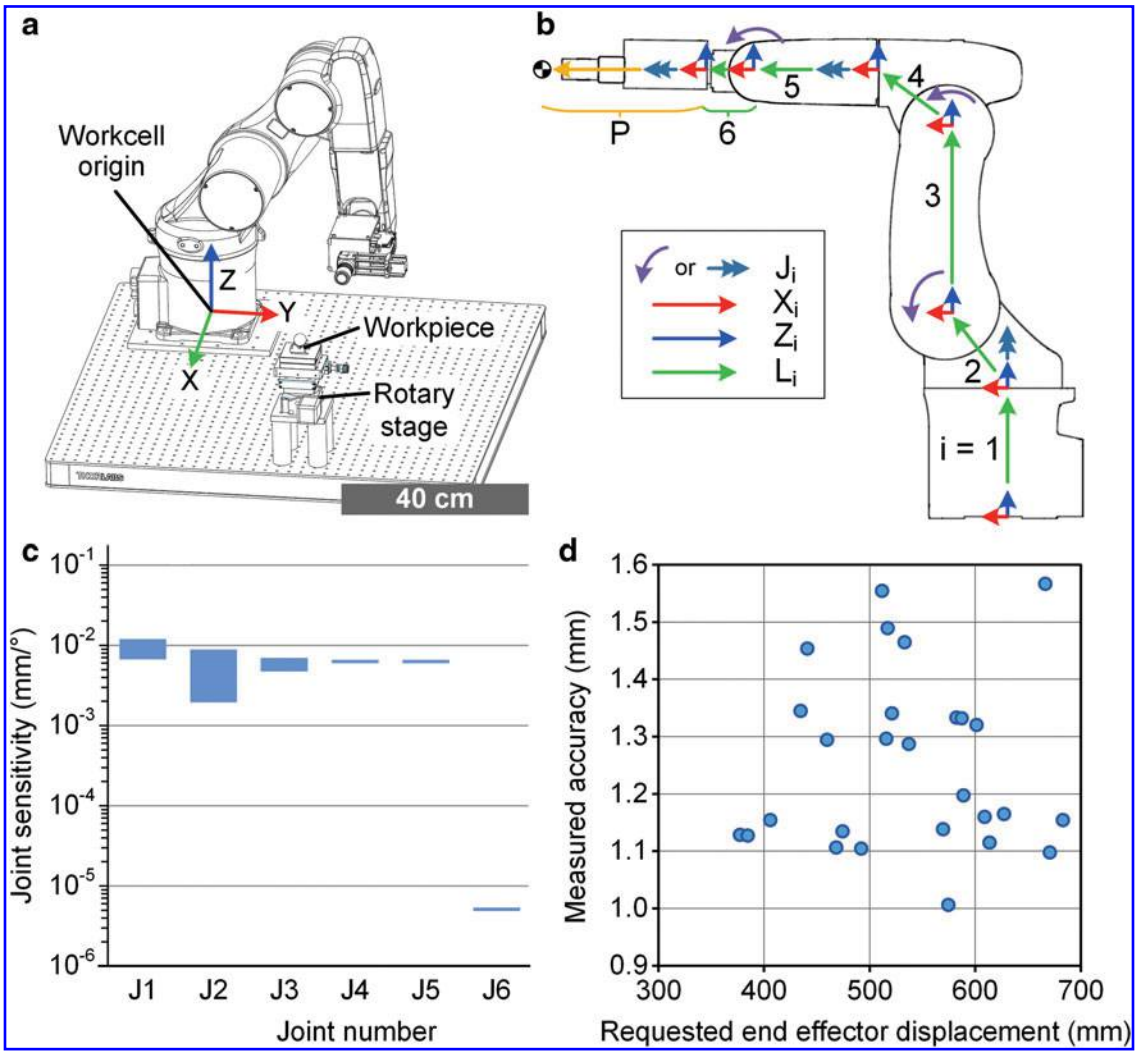

FIG. 3. The performance of the Adept Viper s650 serial articulated robot was analyzed as a key component to the system: **(a)** wireframe of the robot in the workcell in a prototypical pose; **(b)** *side view* of home pose used to construct a kinematic chain model of robot; **(c)** sensitivity contributions of each joint to tool tip position; **(d)** plot of end effector accuracy magnitude (measured via CMM) versus end effector displacement from the robot origin, demonstrating the need for accuracy correction via calibration. CMM, coordinate measuring machine. Color images available online at www.liebertpub.com/3dp

depositing the photopolymer onto the surface of the object, preparing a texture file (Supplementary Fig. S1; Supplementary Data are available online at www.liebertpub.com/3dp) from the 3D scan output, and, finally, exposing sequentially over the entire part and developing the latent photoresist image. To perform 3D patterning (i.e., freeform SLA), this process is repeated incrementally, building away from the workpiece surface. For each exposure, the robot and rotary stage are coordinated to align the projection and cure the photopolymer onto the surface of the part. After all exposures are complete, the workpiece is postprocessed (Supplementary Data).

To facilitate photopatterning on the surface of the 3D object and with nonplanar layers, the workpiece is represented in software by a triangular mesh and is given a pattern through a technique known as UV mapping.[26,27] UV mapping associates each triangle in the mesh with a subsection of a 2D bitmap image described in two dimensions by coordinates (U, V). When rendering the 3D mesh, the subsection of the bitmap associated with each triangle is superimposed on that triangle in the mesh, giving the otherwise featureless 3D mesh geometry a texture. Practically, each triangle is approximately locally parallel to the workpiece and cannot be larger than the field of view of the projector, or further segmentation is required. Figure 4a illustrates the concepts behind UV mapping, starting with an unpatterned geometry, unwrapping that geometry onto a 2D image to associate each triangle with a texture, and finally rewrapping the patterned triangles back into a 3D model. The software, implemented in C++, coordinates the actions of individual hardware subsystems and manipulates and stores the 3D model of the workpiece surface. The rotary stage and DMD system are controlled over USB, and the robot is given commands via Ethernet.

Results

Single-layer robotic photopatterning

For single-layer robotic photopatterning, a layer of photopolymer is applied to the object before initiating the robotic sequence. The polymer is deposited by using an aerosol spray can (Supplementary Data). Subsequently, the robot

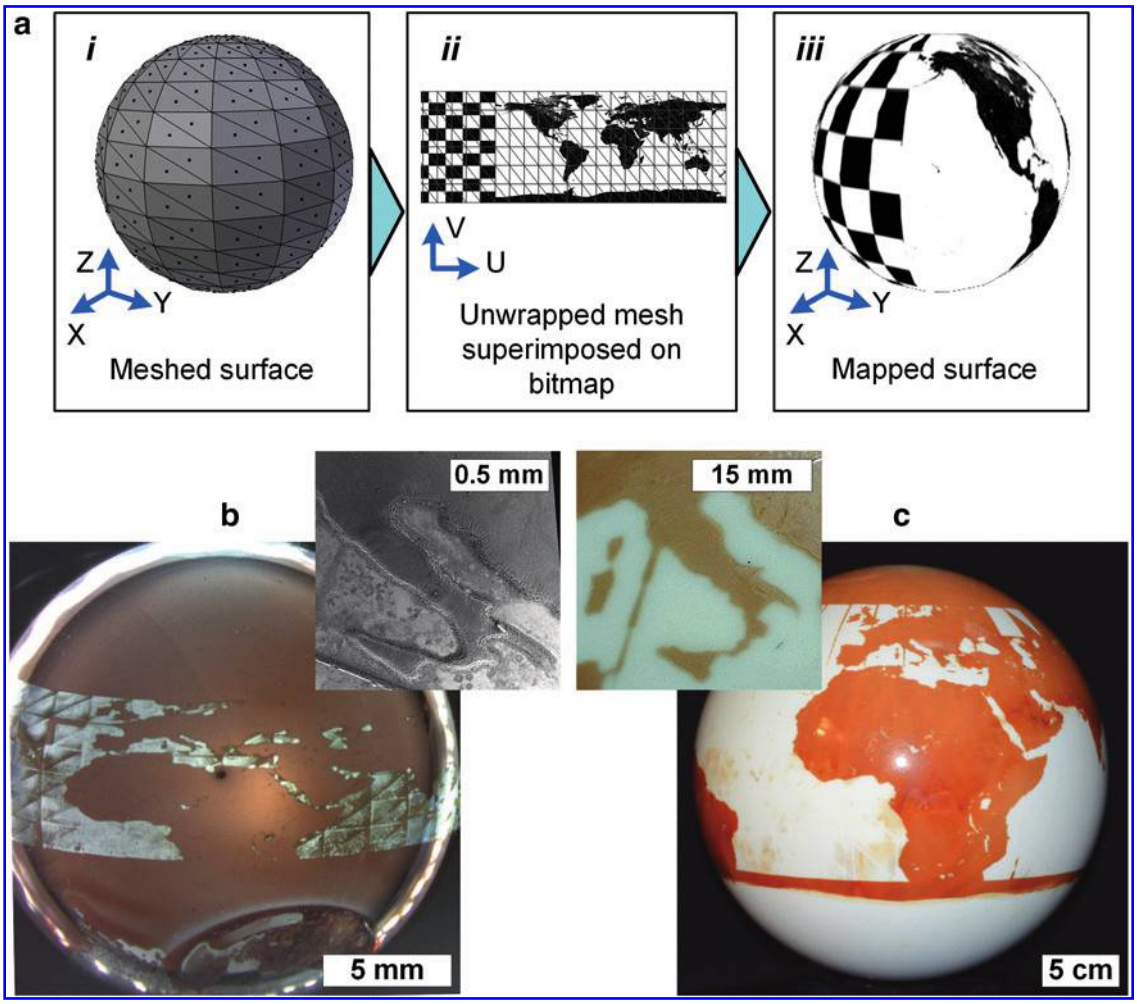

FIG. 4. Demonstration of two-dimensional patterning functionality: **(a)** UV mapping process used to create piecewise digital photomask, here patterning a map onto a sphere with checkerboard region included to clearly show the transformation; **(b)** partial globe map patterned onto 19 mm diameter stainless steel ball bearing using positive photoresist (*inset* shows Italian peninsula); **(c)** partial globe map patterned onto 21 cm diameter polyester sphere using same photoresist (*inset* shows Italian peninsula). Color images available online at www.liebertpub.com/3dp

travels through a series of exposures to tile the complete image along with coordinated motion of the robot arm and rotary stage. To demonstrate this, we chose to pattern an image of Earth onto a spherical workpiece. In Figure 4b (Supplementary Video S1), we show this operation on a stainless steel ball (19 mm diameter); the section of Earth that was patterned comprised 360 triangles and took ~90 min. Earth's landmasses are cured photopolymer, and bodies of water are the substrate that has been revealed by postprocessing. The most significant contribution to the patterning rate is the repositioning time of the motion system between exposures.

In Figure 4c, we show a 21 cm diameter polyester sphere patterned with the same map. For this, a lens system with a larger field of view was installed on the projection lithography end effector. This demonstrates the ability to flexibly increase throughput by increasing the field of vision at the expense of patterning resolution, which was reduced from 10 to 220 μm per linepair. Incidentally, the lower resolution also enabled the operation to be performed without offline CMM calibration of the motion system. Patterning the 21 cm diameter sphere took ~60 h due to the lower light intensity, and correspondingly longer photoresist exposure times (10 min) at the wider field of view.

The same digital mask was used for both the small and large sphere patterning experiments. Defects in inter-triangle spacing in the small sphere map (Fig. 4b) are due to the postcalibration positioning accuracy, whereas the unevenly removed photoresist is due to limited process control of photoresist development. Imperfections in the large sphere map (Fig. 4c) are due to challenges in developing the photoresist on the large sphere, and misalignments between triangles at higher latitudes are due to limited positioning accuracy. Missing triangles are due to software interruption on the system PC.

Stereolithographic AM on freeform surfaces

To characterize and demonstrate nonplanar AM, we first demonstrate the system for conformal photopatterning of single layers on curved surfaces. By modifying the software and end effector hardware, the system can be reconfigured to manufacture 3D structures on freeform substrates. To build multilayer 3D objects, the projection lithography end effector

is modified with an optically transparent window. The gap between the window and surface of the object, determined by the relative position of the robot and workpiece, defines the layer thickness (Supplementary Fig. S2). The software is modified to allow the definition of multiple conformal layers for which a triangulated exposure pattern is determined within each layer. Using commercially available software (Slic3r), the geometric model is sliced in layers that are locally conformal to the substrate surface, and then the triangle pattern is planned. The photopolymer [poly(ethylene glycol) diacrylate, PEG-DA] was replenished manually at the build window before the exposures for each layer.

We show a variety of small objects built on the surface of a sphere (Fig. 5), all with nominal layer thickness of 200 μm and fabrication time of $\sim$20 min. Figure 5a–c demonstrates an additively manufactured millimeter-scale model of the Gateway Arch, a landmark in St. Louis, Missouri, USA. The model consists of 36 separate exposures, with each curved layer printed before advancing to the next layer. At the base of the print, a meniscus of uncured photopolymer is visible. We also built a miniature spiral staircase (Fig. 5d) and a chair with a suspended seat (Fig. 5e). Fabrication of overhanging features such as the stairs and chair seat is enabled by adding UV-absorbing dye (Sudan I, 0.02 wt%) to the photopolymer to limit the depth of cure.

Discussion

The adaptation of robotics to photopatterning and SLA overcomes several important constraints of traditional planar patterning methods. These include the capability for much larger build areas without the bounds of a resin tank, construction on nonplanar objects, and nonplanarity of layers. The patterning and construction of polymers on 3D objects with arbitrary curved surfaces can be used, for example, to decorate parts made by other processes (e.g., injection molding), or to add detailed features that would otherwise require highly complex operations (e.g., texturing of mold surfaces). In general, this concept and workflow can be extended to various manipulator architectures and sizes, and different end effectors could be developed for specific process performance targets.

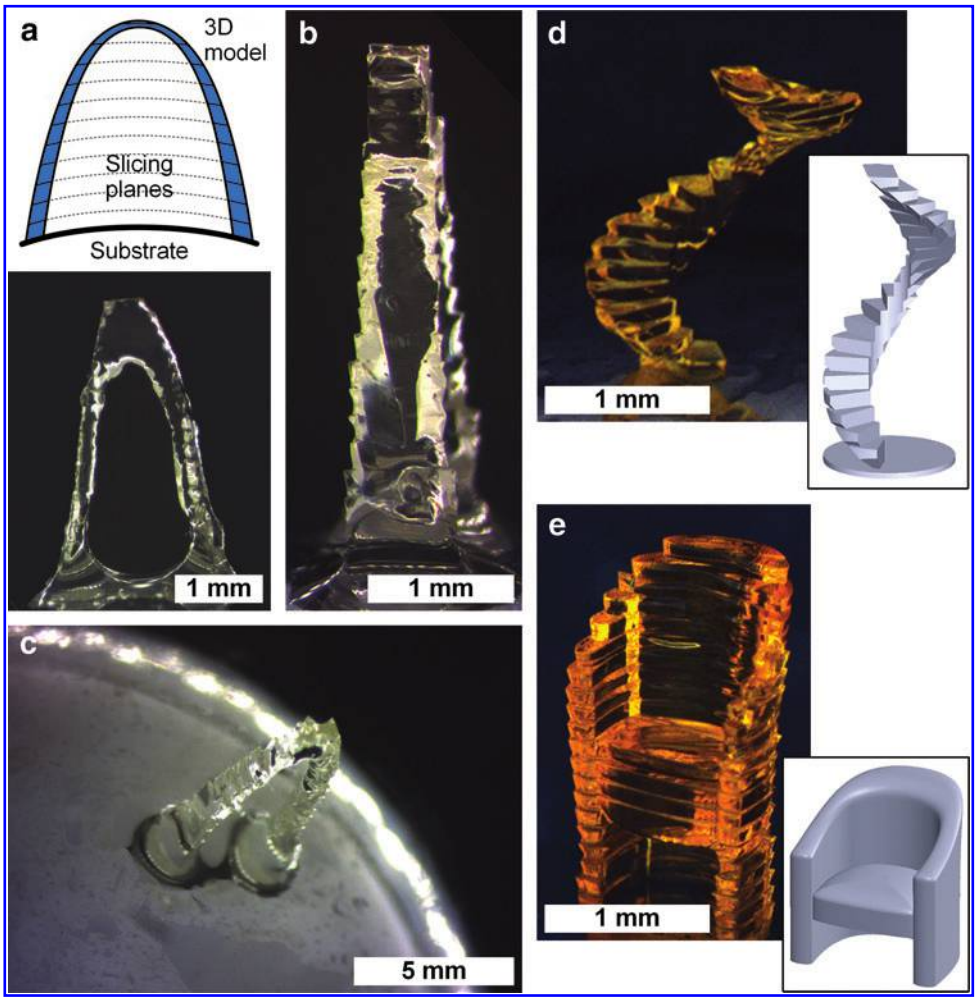

FIG. 5. 3D structures built on curved surfaces by conformal multilayer patterning using the robotic system: **(a)** graphic representation of 3D model showing conformal slicing planes; **(b)** a model of the Gateway Arch (St. Louis, Missouri, USA); **(c)** perspective view of same, showing curved substrate; **(d)** spiral staircase and *inset* of 3D model, demonstrating the ability to print gradually overhanging structures without support material; **(e)** miniature chair with freestanding seat. Color images available online at www.liebertpub.com/3dp

Our study also demonstrates the interdependence of the material deposition process, motion system, and software in determining the process capabilities, including the build resolution and accuracy. In this study, the build fidelity is limited by robot repeatability and accuracy, which was measured at 36 ± 108 and 997 ± 579 μm, respectively. Improving this performance by using a higher accuracy manipulator, and by improved global calibration of the robot, is necessary to build freeform parts with accuracy and surface finish that are comparable to current SLA methods, and to fully utilize the high resolution of the maskless patterning approach. Second, throughput is dominated by the repositioning and settling time of the motion system. For increased throughput, algorithms are needed for continuous motion and exposure as the robot translates. We can also increase the illumination intensity while remaining within the optical limits of the DLP, to increase the photocuring speed. Third, fully automated and robust freeform slicing algorithms would improve part accuracy and surface finish. Fourth and finally, an automated resin delivery system is needed to automate extended build cycles, and to improve the precision of fabricated objects. One such approach would be to connect a syringe pump or pressurized reservoir of photoresin to the end effector by using a flexible tube, and to dispense the photoresin on-demand to match the amount needed with each exposure. Capillary flow between the end effector and the build surface could assist spreading of the resin. Alternatively, the end effector could be augmented with a jetting system to deposit the resin with local dose and composition control.

Conclusion

We have built and demonstrated a robotic system enabling conformal photopatterning on curved surfaces and multilayer additive construction of 3D objects on curved surfaces, with critical dimensions ranging from micrometers to centimeters. We have analyzed the system accuracy and repeatability, and built a digital workflow for patterning on freeform objects via triangulation of the surfaces and automated motion planning of the robot for tile-wise photopatterning. Improved system performance and material development could enable manufacturing of conformal tissue scaffolds for custom medical treatments, nonplanar electronic traces and antennas on and within 3D objects,[5,28] and complex multi-directional parts without the constraints of planar support structures.

Acknowledgments

A.G.S. was supported by the Department of Defense (DoD) through the National Defense Science & Engineering Graduate Fellowship (NDSEG) Program. C.R.O. was supported by the University of Michigan Microfluidics in Biomedical Sciences Training Program through the National Institute of Health (5T32-EB005582), and by the Singapore-MIT Alliance for Research and Technology (SMART). Funding for construction of the lithography system and for materials and characterization was provided by the National Science Foundation (NSF) Scalable Nanomanufacturing Program (DMR-1120187) and by SMART. This work made use of the MRSEC Shared Experimental Facilities at MIT, supported by NSF under award number DMR-1419807. The authors thank Vincent Tiernan and Hexagon Metrology for the use of a Romer 7512 CMM. A.J.H. and C.R.O. conceived the idea. A.G.S. and C.R.O. designed and built the hardware and software, designed and ran experiments, and analyzed data. L.C. designed the enclosure for the rotary stage controller and aided in software design. J.W. designed and built the enclosure for the optical system. M.K. performed error analysis, designed the 3D SLA end effector, and assisted with experiments. A.G.S., C.A., C.B., and J.G. built a first prototype as a project in the ME450 class at the University of Michigan in Fall 2012. E.S.P., C.R.O., and A.J.H. mentored the ME450 team. C.R.O., A.G.S., and A.J.H. wrote the article, with input from all authors. A.J.H. supervised the project.

Author Disclosure Statement

No competing financial interests exist.

References

1. F2792-12a—Standard terminology for additive manufacturing technologies. ASTM International 2013;1–3.
2. Berman B. 3-D printing: The new industrial revolution. Bus Horiz 2012;55:155–162.
3. Frazier WE. Metal additive manufacturing: A review. J Mater Eng Perform 2014;23:1917–1928.
4. Gausemeier J, Echterhoff N, Wall M. Thinking ahead the future of additive manufacturing—Scenario-based matching of technology push and market pull. RTejournal 2012; 9:1–7.
5. Gibson I, Rosen DW, Stucker B. Additive Manufacturing Technologies: Rapid Prototyping to Direct Digital Manufacturing. New York: Springer, 2010.
6. Moore JP, Williams CB. Fatigue properties of parts printed by PolyJet material jetting. Rapid Prototyp J 2015;21:675–685.
7. Seol YJ, Park DY, Park JY, *et al.* A new method of fabricating robust freeform 3D ceramic scaffolds for bone tissue regeneration. Biotechnol Bioeng 2013;110:1444–1455.
8. Eckel ZC, Zhou C, Martin JH, *et al.* Additive manufacturing of polymer-derived ceramics. Science 2016;351:58–62.
9. Zhou C, Chen Y, Yang Z, *et al.* Development of a multimaterial mask-image-projection-based stereolithography for the fabrication of digital materials. In: Annual Solid Freeform Fabrication Symposium. Austin, TX, 2011; pp. 65–80.
10. Wohlers T, Caffrey T. Wohlers Report 2015. Fort Collins: Wohlers Associates, Inc., 2015.
11. Gardner S. Additive Manufacturing and the Factory of the Future. Lockheed Martin Space Systems Company Presentation, 2015.
12. Conner BP, Manogharan GP, Martof AN, *et al.* Making sense of 3-D printing: Creating a map of additive manufacturing products and services. Addit Manuf 2014;1:64–76.
13. Millsaps BB. Voxeljet's VX4000: The largest industrial 3D printer arrives & ready to report to work in North America. 3DPrint.com. Published 2016. https://3dprint.com/131394/voxeljet-vx4000-north-america/ [Accessed June 15, 2016].
14. Barnett E, Gosselin C. Large-scale 3D printing with a cable-suspended robot. Addit Manuf 2015;7:27–44.
15. Ackerman E. Robotic construction gets fancy at ETH Zurich's digital fabrication lab. IEEE Spectr 2016. http://spectrum.ieee.org/automaton/robotics/industrial-robots/robotic-construction-gets-fancy-at-eth-zurich-digital-fabrication-lab (accessed August 28, 2015).

16. Tumbleston JR, Shirvanyants D, Ermoshkin N, *et al.* Continuous liquid interface production of 3D objects. Science 2015;347:1349–1352.
17. Onuh SO, Hon KKB. Optimising build parameters for improved surface finish in stereolithography. Int J Mach Tools Manuf 1998;38:329–342.
18. Pan Y, Chen Y, Zhou C. Fast recoating methods for the projection-based stereolithography process in micro- and macro-scales. In: Annual Solid Freeform Fabrication Symposium. Austin, TX, 2012; pp. 846–862.
19. Calignano F. Design optimization of supports for overhanging structures in aluminum and titanium alloys by selective laser melting. Mater Des 2014;64:203–213.
20. Talagani MR, DorMohammadi S, Dutton R, *et al.* Numerical simulation of big area additive manufacturing (3D printing) of a full size car. SAMPE J 2015;51: 27–36.
21. Holshouser C, Newell C, Palas S, *et al.* Out of bounds additive manufacturing. Adv Mater Process 2013;171: 15–17.
22. Bredt JF, Passino KR. Binder, adhesive and active filler system for three-dimensional printing of ceramics. United States Patent Application #20150315399. Original Assignee: Viridis3D LLC. 2015.
23. Gockel J, Beuth J, Taminger K. Integrated control of solidification microstructure and melt pool dimensions in electron beam wire feed additive manufacturing of ti-6al-4v. Addit Manuf 2014;1:119–126.
24. Adept Viper s650 Technical Data. www.adept.com/products/robots/6-axis/viper-s650/technical-data [Accessed May 30, 2016].
25. Slocum AH. Precision Machine Design. Dearborn, MI: Society of Manufacturing Engineers, 1992.
26. Bogo F, Romero J, Loper M, *et al.* FAUST: Dataset and Evaluation for 3D Mesh Registration. In: The IEEE Conference on Computer Vision and Pattern Recognition (CVPR). IEEE; 2014:3794–3801.
27. OBJ Specification. File Format Info. The Netherlands: University of Twente. www.fileformat.info/format/wavefrontobj/egff.htm [Accessed August 3, 2016].
28. Moonen PF. Alternative lithography strategies for flexible electronics. 2012.

Address correspondence to:
A. John Hart
Department of Mechanical Engineering and Laboratory for Manufacturing and Productivity
Massachusetts Institute of Technology
77 Massachusetts Avenue
Cambridge, MA 02139

E-mail: ajhart@mit.edu